Plasma Wave Generation in a Self-Focused Channel of a Relativistically Intense Laser Pulse

C. E. Clayton,[1] K.-C. Tzeng,[1] D. Gordon,[1] P. Muggli,[1] W. B. Mori,[1] C. Joshi,[1] V. Malka,[2] Z. Najmudin,[3] A. Modena,[3] D. Neely,[4] and A. E. Dangor[3]

[1]*UCLA Department of Electrical Engineering, Los Angeles, California 90095*
[2]*LULI Laboratory, CNRS-Ecole Polytechnique, Palaiseau, France*
[3]*Blackett Laboratory, Imperial College, London SW7 A2Z, United Kingdom*
[4]*Central Laser Facility, Rutherford Appleton Laboratory, Didcot, United Kingdom*

(Received 1 July 1997)

Evidence for self-channeling of a relativistically intense laser pulse in an underdense plasma is presented through Schlieren and 90° Thomson sidescatter images. Using collective Thomson scattering of a probe beam, we observe that relativistically propagating plasma waves are excited over the entire length of the channel, up to 12 Rayleigh lengths (≈4 mm). From the wave amplitude, the intensity inside the channel is estimated to be $\sim 10^{18}$ W/cm^2. [S0031-9007(98)06554-5]

PACS numbers: 52.40.Nk, 41.75.Lx, 52.35.Mw, 52.60.+h

A powerful laser pulse, when focused in a plasma, can propagate a distance greater than the Rayleigh length x_R (the distance in which the intensity of a laser beam focused in vacuum drops a factor of 2) through ponderomotive and relativistic self-focusing [1]. This ability to extend the interaction length is crucial to various x-ray laser [2], plasma accelerator [3], and fast ignitor fusion schemes [4]. Self-focusing results from an increase of the on-axis index of refraction relative to the edge of the laser beam through depressing the on-axis electron density (ponderomotive self-focusing) or through the radially dependent relativistic correction to the plasma frequency when the quiver velocity of the electrons in the laser field becomes relativistic (relativistic self-focusing), or both. These self-induced alterations of the plasma refractive index can allow the laser to self-focus and/or filament into several beamlets [5]. Although there is a threshold power condition for self-focusing to occur [1], the accompanying effects of high intensity such as electron plasma wave (EPW) generation [6,7], electron acceleration [8,9], and plasma heating [10] may influence how the channel ultimately behaves. Previous work has demonstrated that psec laser pulses are indeed self-guided under appropriate conditions [11]. The work reported in this Letter extends this knowledge base by explicitly showing that relativistically propagating plasma waves are excited inside—and over the entire length of—a self-channeled laser beam. Estimates of the amplitude of these EPW's suggest that the channeled laser intensity is $\sim 10^{18}$ W/cm^2 over a distance of up to 12 Rayleigh lengths.

The experiment (see Fig. 1) was performed at the Central Laser Facility at the Rutherford Appleton Laboratory. One beam of the Vulcan laser (the "pump") provided up to 20 J of $\lambda_0 = 1.055$ μm light in a 1 psec FWHM pulse [12] and was focused with an $f/4.5$ off-axis parabola to a spot diameter containing 85% of the laser energy in about 20 μm with an $x_R \approx 350$ μm. The vacuum intensity was about 5×10^{18} W/cm^2 corresponding to a normalized vector potential $a_0 = eA/mc^2 \approx 2$. Other relevant parameters are plasma density $n_e = 1.7\text{–}2.0 \times 10^{19}$ cm^{-3} and laser power $P \approx 20$ TW corresponding to 20–24 P_{cr}, where $P_{cr} \approx 1.7 \times 10^{19}/n_e$ TW is the critical power for relativistic self-focusing of 1 μm light. A frequency-doubled probe beam (≈20 psec full width at 10% maximum) was used for the Thomson scattering and Schlieren photography. The focal point of the horizontally polarized (y direction in Fig. 1) pump was placed at the sharp front edge of a 4 mm diameter supersonic

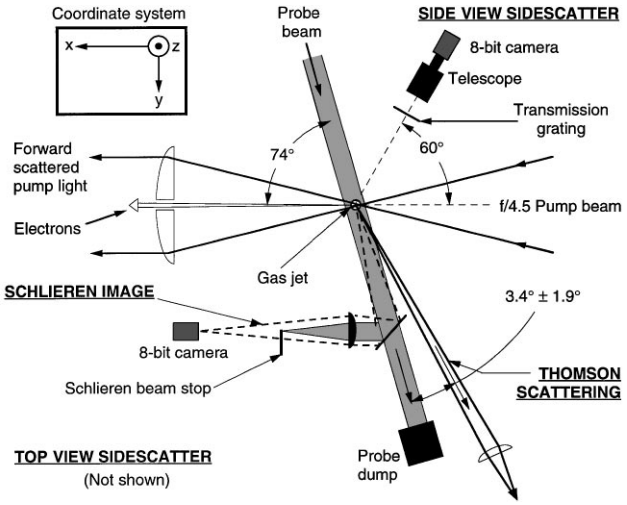

FIG. 1. Experimental setup shown schematically. The center of the jet is at $x = 0$ and the laser was focused at $x \approx -2$ mm, propagating in the $+x$ direction. Three imaging diagnostics lie in the x-y plane while the top-view sidescatter imaging setup (not shown) looks along the negative z direction. The forward-scattered pump light was collected in the forward $f/4.5$ cone and the electrons were collected in a $f/100$ cone defined by a thick collimator (not shown). The collective Thomson scattering from the probe beam was imaged onto the slit of an imaging spectrograph with a one ns gated "image intensifier" (gain ~100) at the output plane. The spatial resolution along the slit was ≈150 μm while the spectral resolution was ≈64 Å.

 0031-9007/98/81(1)/100(4)$15.00

plume of helium gas, 2 mm above the jet body. Forward-scattered pump light was spectrally analyzed as were forward-going electrons.

The image of the sidescattered pump light shown in Fig. 2(a) shows two distinct filaments extending roughly 10 Rayleigh lengths from the laser focus at $x = -2$ mm to $x \approx 1.5$ mm while in the orthogonal plane [Fig. 2(b)] only one filament extending out to $x \approx 1.5$ mm is apparent. The transverse size of the individual filaments is not resolved. Analysis of these images from all the shots shows that typically one or two filaments would survive beyond $x = -1$ mm (in both views, but not symmetrically) and on several shots, a dominant filament would itself split into two, well beyond $x = -1$ mm. This is not surprising for a beam with an initial $P/P_{\mathrm{cr}} \gg 1$ which is highly unstable to "filamentation" [5]. Figure 2(c) shows the Schlieren image taken during this laser shot. There are two "whiskers" of exposure due to the refractive index gradients at the edges of the two light-guiding channels seen in Fig. 2(a) confirming refractive-index guiding out to, again, $x \approx 1.5$ mm. The inside dimensions of the cone-shaped feature in the Schlieren image nearly matches the $f/4.5$ vacuum divergence of the ~flat-topped laser beam (10 cm vertical and 8 cm wide). The observed refractive index gradients at the exit of the gas plume ($x \approx 2$ mm) correspond to the He I/He boundary which requires an intensity of about 10^{15} W/cm^2 [13] implying a peak power of >6 TW when evaluated 4 mm from the focus. Clearly, not all of the 20 TW laser pulse was captured into the two filaments on this shot. Also, the $\sim f/4.5$ cone of the plasma and lack of density gradients at larger angles implies that ionization-induced refraction, although possibly playing a role in the coupling of laser light into filaments, has not refracted substantial laser power into large cone angles [14].

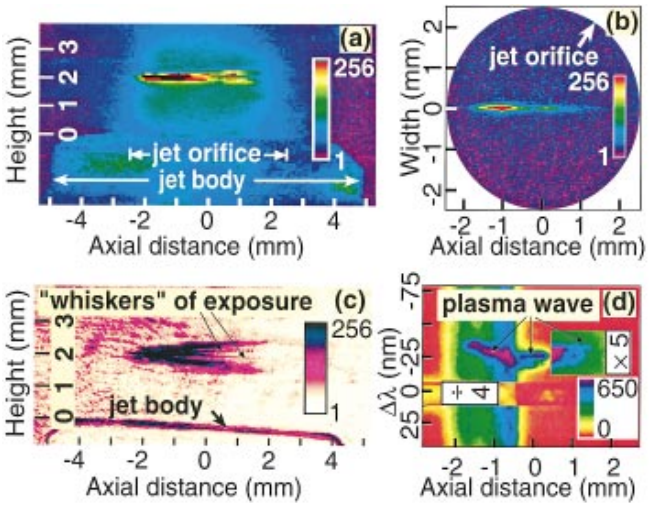

FIG. 2(color). Results from all four imaging diagnostics taken on the same laser shot with $P \approx 20$ TW and $n_c/\gamma \approx 1.4 \times 10^{19}$ cm^{-3}. Axial distance represents position along the laser axis. (a) Side-view sidescatter near 1 μm. (b) Top-view sidescatter taken through a near-infrared glass filter. (c) Schlieren image taken with the probe beam. (d) Time-integrated (20 ps probe pulse and 1/2 ns optical gate) raw-data image from collective Thomson scattering. The region between $0.4 < x < 1.8$ mm was multiplied by 5 in the image file while stray light near $\Delta\lambda = 0$ was divided by 4.

Figure 2(d) shows data from collective Thomson scattering of the probe beam off EPW's in a channel, collected with $f/15$ optics. Here, as in Fig. 3(a), $\Delta\lambda$ is the wavelength shift from the probe beam wavelength. The near transverse probe beam is k matched to EPW modes centered around $\mathbf{k} = k_p\hat{\mathbf{x}} \pm k_\perp\hat{\mathbf{y}}$ where $k_\perp/k_p \sim 1$, k_p is the wave vector of the EPW in the laser direction (see Fig. 1), and $\hat{\mathbf{x}}$ and $\hat{\mathbf{y}}$ are the unit vectors. These two modes fall easily within the k spectrum of the relativistic EPW since the spot size of the laser is on the order of the plasma wavelength λ_p [15]. Note that while each mode by itself is nonrelativistic, their superposition is a relativistic EPW with transverse spatial structure [16]. Because of the symmetry imposed by the laser beam and/or the channel, both modes must be present, and indeed, the mode at $-k_\perp$ is seen in the Thomson scattering as a blueshifted feature which is a perfect "mirror image" about the probe frequency of the redshifted feature. However, because of the ≈2.5° difference in scattering angle (on the order of the angle subtended by the collection lens), the optics vignette the blue satellite thereby reducing its intensity relative to the red satellite shown.

The diagnostic will obviously pick up signals from any modes centered around $\mathbf{k} = k_p\hat{\mathbf{x}} \pm k_\perp\hat{\mathbf{y}}$ regardless of their origin. Besides resulting from the finite transverse extent of the relativistic EPW, such modes might arise from Raman sidescatter. However, the limited interaction length and low noise sources for this instability makes it unlikely that such modes would grow to a substantial level. At the same time, substantial sidescattered radiation is inferred in the experiment and seen in PIC simulations. This radiation arises predominantly from two phenomena. First, the EPW propagating with the pump focuses and defocuses the light at density minima and maxima, respectively, resulting in a transverse modulation in the EPW driving force [17]. Second, the plasma wave itself will distort to both its amplitude-dependent frequency [18] and the effect of the channel which lowers the EPW frequency on axis relative to off axis. These effects add to cause curving of the EPW phase fronts, enhancing the plasma wave k-spectral intensity near $k_\perp \sim k_p$ and thus scattering light out conically at an angle of about $k_\perp/k_0 \sim 0.14$ or 8°, where k_0 is the wave vector of the laser beam.

There are two distinct features present in the image of Fig. 2(d) and on all other shots: (1) broadband light from the plasma itself due to bremsstrahlung continuum emission covering all frequencies near $2\omega_0$ and present even when the probe beam is blocked, though not necessarily uniform along the x direction; and (2), probe

light scattered by relativistic EPW's within a channel and frequency shifted by the effective plasma frequency $\omega_p/\gamma^{1/2}$. Here γ is the relativistic Lorentz factor due to the plasma electrons quivering in the transverse field of the laser. In Fig. 2(d), this EPW image begins about 220–250 μm from the laser focus at $x = -2.0$ mm, persists as a bright feature for about 2.4 mm to $x \approx 0.4$ mm, and then continues at roughly 5 $\times$ lower brightness out to $x \approx 1.5$ mm. The 200–250 μm gap between the laser focus and the first observable EPW signature, characteristic of all data shots, is in reasonable agreement with the growth rate of the Raman forward scattering (RFS) instability [6].

In Fig. 2(d) the sudden drop of the bremsstrahlung continuum at $x \approx -0.3$ mm is probably due to the intensity of the untrapped laser light dropping through the threshold intensity $I_{\mathrm{He\ II}}$ for producing He II of about 10^{16} W/cm^2. Since bremsstrahlung emission scales as $Zn_e^2 w(x)$ [19], which drops a factor of 8 at the He II/He I boundary, its signal changes abruptly. This implies that the uncaptured power $P_1 = A(-0.3\ \mathrm{mm})I_{\mathrm{He\ II}} \approx 11$ TW for the flat-topped beam diverging at $f/4.5$ with an area A. There is also a drop in, and a broadening of, the apparent plasma frequency as one moves towards the center of the jet. Three possible contributions to the ω_p reduction are (1) the unperturbed neutral profile of the gas jet; (2) self-focusing leading to an increase of γ, and (3) ponderomotive blowout leading to a drop in n_e. An ω_p measurement from a low power (3 TW) shot with the laser focused at the center of the jet indicated that the upper boundary of $\omega_p(x)$ is probably due to the neutral-gas pressure variation across the jet. Contributions to broadening of ω_p are (1) transient changes in n_c/γ as the laser intensity rises and falls at each point in space; or (2) at a given time, the probe is scattering off EPW's with a range of frequencies as might occur on the walls of a deep channel. Both of these possibilities require similarly high laser intensities (10^{18}–10^{19} W/cm^2) for psec long pulses. A final feature to note is that the Thomson scattering suddenly drops about a factor of 5 at $x \approx 0.4$ mm. This is probably because the filament is not necessarily aligned parallel to the slit of the spectrometer (x direction) and the image can therefore "walk off" the slit. We have observed shot-to-shot variations in the precise direction that filaments form in the x-y plane attributable to either shot-to-shot variations in the focal spot quality or jitter in the boundary of the gas jet. On some shots where a single filament was observed close to the laser beam axis, the filament and the plasma wave were indeed seen to exist throughout the $\approx$4 mm length of the gas jet plume corresponding to about $12x_R$.

An example of this is shown in Fig. 3. The plasma wave is shown in Fig. 3(a), whereas the corresponding 90° sidescatter image is shown in Fig. 3(b). One can see axial correlations between the intensely emitting regions of sidescatter and EPW activity. This argues against total

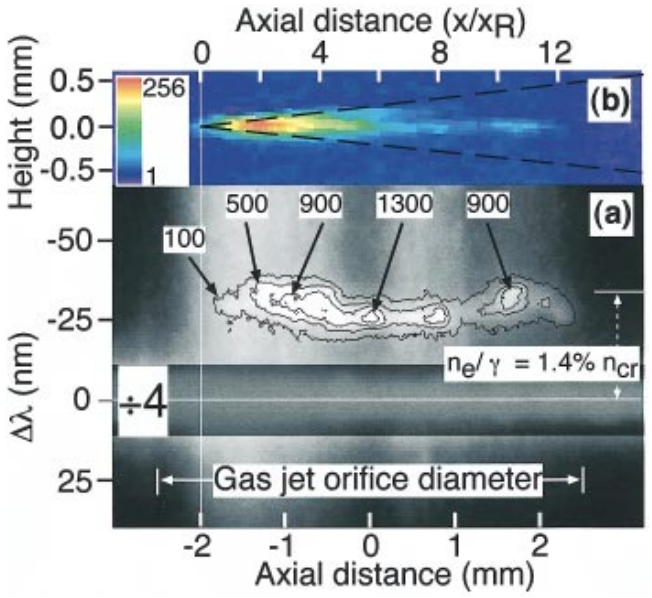

FIG. 3(color). Results from two imaging diagnostics from the same laser shot with $P \approx 20$ TW and $n_c/\gamma \approx 1.4 \times 10^{19}$ cm^{-3}. Axial distance represents position along the laser axis. (a) Time-integrated (20 ps probe pulse and 1/2 ns optical gate) raw-data image from collective Thomson scattering. Contours of constant scattered energy were obtained by subtracting the average bremsstrahlung background at each spatial location and applying the contours to the resultant Thomson-scattering-only image. The effective plasma density is labeled in terms of the critical density (n_{cr}) for the pump frequency. Stray light near $\Delta\lambda = 0$ was divided by 4 in the image file. (b) (color) Side-view sidescatter image dominated by light near 1 μm. Dashed lines represent the $f/4.5$ focal cone of the laser in vacuum.

electron cavitation [20], predicted to occur where the sidescatter is brightest [21], since ω_p and therefore the density is substantial at these points and throughout the filament. The density fluctuation levels $\tilde{n}/n$ associated with EPW's in Figs. 2(d) and Fig. 3(a) were estimated to within a factor of 3 in the following way. On other shots where >90 MeV electrons were observed and the EPW image was very short and uniform in frequency, a calibration could be made between counts on the CCD camera which viewed the Thomson scattering and the implied average electric field of $\sim$160 GeV/m. The estimate for $\tilde{n}/n$ in this case was 20%–60%. The definitive lower bound assumes coherent electron acceleration to 94 MeV over the observed 600 μm extent of the EPW without any phase slippage. The more reasonable upper bound comes from signatures of wave breaking in the forward scattered spectrum [8] and is consistent with wave breaking levels observed in 2D PIC simulations. For the shots shown in Figs. 2(d) and 3(a), the maximum CCD count level was comparable to the above-mentioned calibration shot while the electron spectrum extended to only about 70 MeV in Fig. 2 and about 90 MeV in Fig. 3. We believe that the EPW amplitudes are indeed in the 20%–60% range but

that the acceleration (numbers of electrons at each energy and maximum observed energy) may have been adversely affected by the density-, intensity-, and therefore phase-velocity-nonuniformities over the length of the gas jet.

Computer simulations, even in a homogeneous density plasma, show that different physical mechanisms excite the plasma wave at different locations across the plasma. Self-modulation of the initially smooth laser intensity envelope occurs as RFS grows in the first few 100 μm of the gas plume [17,22]. The finite exponentiation length of this instability is implied in the aforementioned 200–250 μm gap between the laser focus and the first observable EPW (with $\tilde{n}/n_e$ already $>10\%$) in the experiment. Thereafter, although the front of the laser pulse propagates into fresh plasma, the envelope is continuously and irreversibly modulated both longitudinally and transversely and the theoretical model of RFS no longer applies. In addition to RFS, Raman backscatter, the previously discussed sidescatter, and relativistic self-phase modulation [1] can locally scatter light into a range of angles, eroding away portions of the laser envelope, especially in the rising edge. After one or two Rayleigh lengths, the longitudinal scale lengths of the intensity variations are on the order of λ_p, and the modulations can directly drive EPW's through the plasma wake field effect [17,22].

From Fig. 3(a), there is a roughly 40% wave at $x = 1.7$ mm which has been driven up even though the frequency has changed by 25% from $x = 1$ mm, thus precluding any resonant excitation process. The minimum intensity needed to drive this wave level can be found from the nonlinear, 3D wake field formulism [3]

$$\frac{\tilde{n}}{n_e} \approx \frac{a_1^2/2}{(1 + a_1^2/2)^{1/2}} \times \left[1 + \frac{8}{k_p^2 w^2}\left(1 - \frac{2r^2}{w^2}\right)\right]\exp\left[\frac{-2r^2}{w^2}\right], \quad (1)$$

where a_1 is the local-maximum in the vector potential of the envelope modulation that is driving the wave, and the r or radial dependence arises from the assumption that the channeled pulse has a Gaussian profile of spot size w. A particular longitudinal shape to the modulation "bump" was assumed, but the result is fairly insensitive to the exact shape. There are two constraints that we can apply before we derive an estimate of a_1. First, since Eq. (1) contains both the laser intensity and beam area, any choice of (a_1, w) implies a particular instantaneous power P_0 within the filament or channel. From the earlier discussions, up to 9 TW appears to be available for this channel whereas self-channeling requires $P_0/P_c > 1$ TW suggesting numerical values for (a_1, w) in Eq. (1) be constrained such that $1 < P_0 < 9$ TW. This leads to a minimum-required intensity of $0.5–1.8 \times 10^{18}$ W/cm^2 at $r = 0$ and channel radii in the range $w = (6.3–14)k_p^{-1}$ or 7.5–17 μm for EPW amplitudes of (20–60)%.

The authors would like to thank C. Danson at the Vulcan Laser Facility and his staff for excellent user support. This work was supported by EPSRC Grants No. GR/J90770 and No. GR/L26636, the EU, the Laboratoire Europeen Associé LULI/DRAL and the U.S. Department of Energy under Contract No. DE-FG03-92ER40727.

[1] C. E. Max *et al.*, Phys. Rev. Lett. **33**, 209 (1974); P. Sprangle *et al.*, IEEE Trans. Plasma Sci. **15**, 145 (1987).
[2] N. H. Burnett and G. D. Enright, IEEE J. Quantum Electron. **26**, 1797 (1990).
[3] E. Esarey *et al.*, IEEE Trans. Plasma Sci. **24**, 252 (1996).
[4] M. Tabak *et al.*, Phys. Plasmas **1**, 1626 (1994).
[5] F. Vidal and T. W. Johnston, Phys. Rev. Lett. **77**, 1282 (1996).
[6] W. B. Mori *et al.*, Phys. Rev. Lett. **72**, 1482 (1994), and references therein.
[7] T. Tajima and J. M. Dawson, Phys. Rev. Lett. **43**, 267 (1979).
[8] A. Modena *et al.*, Nature (London) **377**, 606 (1995).
[9] C. A. Coverdale *et al.*, Phys. Rev. Lett. **74**, 4659 (1995); D. Umstadter *et al.*, Science **273**, 472 (1996); C. I. Moore *et al.*, Phys. Rev. Lett. **79**, 3909 (1997).
[10] D. W. Forslund *et al.*, Phys. Rev. Lett. **54**, 558 (1985); J. N. Bardsley *et al.*, Phys. Rev. A **40**, 3823 (1989).
[11] A. B. Borisov *et al.*, Phys. Rev. Lett. **68**, 2309 (1992); P. Monot *et al.*, Phys. Rev. Lett. **74**, 2953 (1995); K. Krushelnick *et al.*, Phys. Rev. Lett. **78**, 4047 (1997); R. Wagner *et al.*, Phys. Rev. Lett. **78**, 3125 (1997).
[12] C. N. Danson *et al.*, Opt. Commun. **103**, 392 (1993); C. Danson *et al.*, in Proceedings of the 24th ECLIM, Madrid, 1996 (to be published).
[13] S. Augst et al., J. Opt. Soc. Am. B **8**, 858 (1991).
[14] T. Auguste *et al.*, Opt. Commun. **97**, 292 (1994); C. D. Decker *et al.*, Phys. Plasmas **3**, 414 (1996).
[15] A. Lal *et al.*, Phys. Plasmas **4**, 1434 (1997).
[16] Consider that $\cos(k_p x + k_\perp y - \omega_p t) + \cos(k_p x - k_\perp y - \omega_p t) = \cos(k_\perp y)\cos(k_p x - \omega_p t)$.
[17] C. D. Decker *et al.*, Phys. Rev. E **50**, R3338 (1994); C. D. Decker *et al.*, IEEE Trans. Plasma Sci. **24**, 379 (1996).
[18] S. V. Bulanov *et al.*, Phys. Rev. Lett. **74**, 710 (1995).
[19] J. Dawson and C. Oberman, Phys. Fluids **5**, 517 (1962).
[20] G.-Z. Sun *et al.*, Phys. Fluids **30**, 526 (1987).
[21] P. Gibbon *et al.*, Phys. Plasmas **2**, 1305 (1995).
[22] K.-C. Tzeng *et al.*, Phys. Rev. Lett. **76**, 3332 (1996).